Research Article | Vol. 33, No. 10 / 19 May 2025 / Optics Express 21173
Optics EXPRESS

Simultaneous observation of bright and dark polariton states in subwavelength gratings made from quasi-bulk WS_2

PAUL BOUTEYRE,[1,3] XUERONG HU,[1] SAM A. RANDERSON,[1] PANAIOT G. ZOTEV,[1] YUE WANG,[2] AND ALEXANDER I. TARTAKOVSKII[1,4]

[1]School of Mathematical and Physical Sciences, University of Sheffield, Sheffield S3 7RH, UK
[2]School of Physics, Engineering and Technology, University of York, York YO10 5DD, UK
[3]p.bouteyre@sheffield.ac.uk
[4]a.tartakovskii@sheffield.ac.uk

Abstract: Over the last decade, layered crystals, referred to as van der Waals (vdW) materials, have attracted tremendous interest due to their unique properties in their single and few layer forms. Their bulk counterparts, however, have only been recently explored as building blocks for nanophotonics. Indeed, bulk vdW materials offer promising properties such as high refractive indices and adherence to any type of substrate. We present here a variety of 1D grating structures composed of bulk transition metal dichalcogenide (TMD) WS_2 as a highly tunable and versatile platform for observation of a multi-level polaritonic system. The WS_2 excitons are simultaneously strongly coupled with the two grating photonic modes, including the bound state in the continuum (BIC) of the lower energy mode, giving rise to polariton-BICs. The polaritonic dispersion shapes can be varied in a straightforward fashion by choosing WS_2 films of different thicknesses and changing the gratings periods.

1. Introduction

Exciton-polaritons [1], half-light half-matter quasiparticles, arise from the strong coupling regime between an excitonic and a photonic state when the coupling rate between the two states is faster than the respective dissipation rates. Exciton-polaritons have been demonstrated in many nanofabricated photonic strutures such as microcavities [1–3], photonic crystals [4–15] or micropillar lattices [16–18]. From their hybrid nature, the exciton-polaritons hold the properties of their light and matter counterparts, and therefore are nonlinear bosons that can propagate ballistically. Using these properties, many proof-of-concept polaritonic devices, potential candidate for future all-optical devices, were demonstrated [2,19–23]. Moreover, thanks to the excitonic part of polaritons, several nonlinear effects were reported [4–6,8,9,15–18], such as polaritonic lasing [3,5,6,9,16,17] or few-photon all-optical phase rotation [18].

Topological properties of exciton-polaritons were also explored using topological photonic structures [11,16,17,24], while non-Hermitian properties were studied in the strong coupling between semiconductor excitons and Bound States in the Continuum (BIC) in photonic structures giving rise to the so called polariton-BICs [4–7,9–12,14,15]. The symmetry-protected BICs [25,26] with intriguing non-Hermitian properties [27] are dark photonic states forbidden to couple to the continuum spectrum of radiation outside a confined photonic structure. They occur due to destructive interference in the far field between the continuum of radiation and an asymmetric photonic mode stemming from the photonic structure symmetry.

#553437 https://doi.org/10.1364/OE.553437
Journal © 2025 Received 20 Dec 2024; accepted 10 Apr 2025; published 12 May 2025

Optics EXPRESS

In the meantime, layered crystals, dubbed van der Waals (vdW) materials, have over the last two decades attracted tremendous interest due to their unique properties in their single and few layer forms. Indeed monolayers of diverse 2D materials, especially of transition metal dichalcogenides (TMDs), possess robust excitons accessible at room temperature in contrast to III-V quantum wells. For these reasons, monolayers of vdWs materials have been integrated in various silicon, silicon nitride, or III-V semiconductor based photonic structures ranging from polaritonic devices in microcavities [28], to polaritons in Spin-Hall topological lattices [29].

The bulk counterparts of these 2D materials, have been less explored for potential use in nanophotonics as the direct bandgap of TMDs becomes indirect in the multilayer form, which considerably reduces their quantum yield. However, bulk 2D materials offer very attractive properties for realizing photonic building blocks. Similarly to monolayers, they can be readily fabricated via mechanical exfoliation and they adhere easily to a wide range of substrates without the need for chemical bonding or lattice matching. It was also recently shown that standard lithography can be used to pattern 2D materials leading to high quality structures [30,31]. As bulk materials, TMDs show relatively low absorption in the near-infrared (for wavelengths above 700 nm for the case of WS_2), which according to several recent ellipsometry studies [32–34] is much lower or comparable to absorption in silicon. Combined with high refractive indices exceeding 4, this makes TMDs promising for waveguides as was recently demonstrated for MoS_2 [35].

Exciton-polaritons were observed in bulk WS_2 photonic crystals in which the TMD served both as the excitonic material and building block of the photonic structure [34,36–38]. Indeed, bulk WS_2 has a direct local bandgap (as opposed to the global bandgap) at the K point and still exhibits strong excitons [34,37]. Propagation of exciton-polaritons as well as hybrid exciton-plasmon-excitons were studied in bulk WS_2-based gratings [13,39]. However, the configurations of these structures were such that the non-Hermiticity of the photonic system such as the strong coupling between the WS_2 exciton and the grating BICs could not be explored. Moreover, the WS_2 excitons were strongly coupled to only one of the grating modes.

In this context, we present here a highly tunable and versatile platform for observation of a double polaritonic system based on a bulk van der Waals excitonic material. We realize a variety of 1D grating structures composed of transition metal dichalcogenide WS_2 multilayers of thicknesses 10 to 60 nm on SiO_2 and Au substrates with respective grating periods of 350 nm and 400 nm and filling factors 0.55 and 0.7. The WS_2 excitons are simultaneously strongly coupled with the two grating photonic modes including the BIC of the lower energy mode giving rise to polariton-BICs (pol-BICs). The polaritonic dispersions shapes can be varied in a straightforward fashion by choosing WS_2 films of different thicknesses and by changing the period of the grating.

The combination of advantages of 2D materials and of polaritons in a highly tunable and versatile platform, opens the way to a new prospect of future polaritonic photonic devices. Indeed, it was proposed that entire photonic circuits could be made of TMDs [40]. Moreover, the highly tunable subwavelength gratings presented in our work could also be used in conjunction with slabs and whole photonic structures made from van der Waals or many other materials such as III-V membranes placed on top, thus opening the way to 3D nanophotonic heterointegration and straightforward fabrication of sophisticated polaritonic devices.

In the following, we will first describe the double polaritonic system by performing RCWA (Rigorous Coupled Wave Analysis) simulations of a suspended grating of refractive index close to that of WS_2. Finally, we will experimentally demonstrate the double polaritonic system in WS_2-based gratings on SiO_2/Si and Au substrates in angle-resolved reflectivity measurements.

2. Model and numerical results

To understand the double exciton-polariton system, let us first consider the uncoupled photonic modes in a suspended grating (see Fig. 1(a)) of refractive index of 4.5 (close to the average

Optics EXPRESS

refractive index of WS_2 at around 2 eV), and with a zero extinction coefficient. The grating consists of a single slab periodically etched along the x direction in wires extending in the y direction, and is characterized by its thickness, t, period a, and filling factor FF. The two uncoupled photonic modes, E_{ph1} and E_{ph2}, of this structure result from the band folding and diffractive coupling of TE modes propagating along the x direction within the grating slab, and are described by (more details in Supplement 1, section 2):

$$E_{ph1,ph2}(k_x) = E_0 \pm \sqrt{U^2 + (v_g^{ph1,ph2} k_x)^2} \tag{1}$$

where U is the coupling strength of the diffractive coupling, E_0 the mid-gap energy, and $v_g^{ph1,ph2}$ the group velocity of each of the modes. As shown in Fig. 1(a), these two parabolic-like dispersions separated by a gap of $2U$ can be observed in RCWA (Rigorous Coupled Wave Analysis) reflectivity simulations (more details in Supplement 1, method section) of a suspended grating (a=360nm, FF=0.8 t= 20nm, n=4.5), where U=255 meV, E_0=1.98 eV, v_g^{ph1}=72 meV.μm, v_g^{ph2}=62 meV.μm. Note that the low-energy photonic mode, E_{ph1}, vanishes when approaching zero momenta k_x. This dark state occurs due to destructive interferences induced by the in-plane symmetry of the photonic crystal and corresponds to a Bound State in the Continuum (BIC) [25,26].

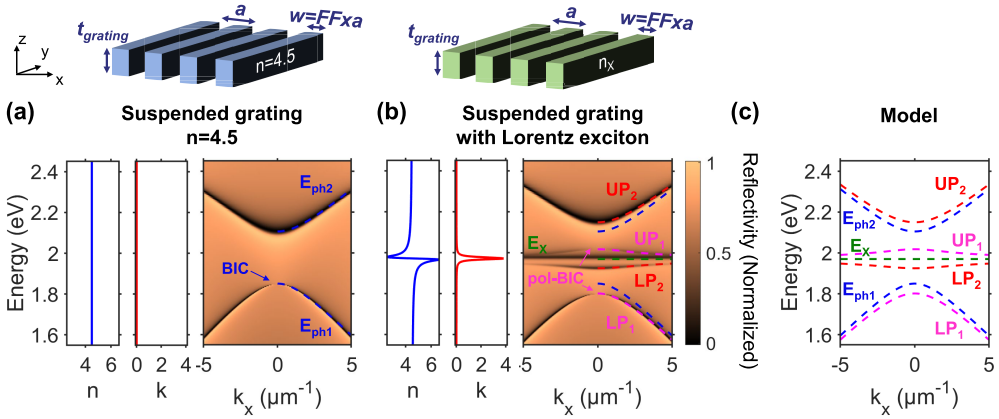

Fig. 1. Analytical model on simulated suspended gratings. (a) Simulated reflectivity performed with rigorous coupled wave analysis (RCWA) of a suspended grating (a=360 nm, FF=0.8 t=20 nm) with a constant refractive index with no losses (n=4.5, k=0). The two photonic modes of the grating, E_{ph1} and E_{ph2}, are fitted with Eq. (1) (U=255 meV, E_0=1.98 eV, v_g^{ph1}=72 meV.μm, v_g^{ph2}=62 meV.μm), and are depicted by blue dash lines. A bound state in the continuum (BIC) can be observed on the lower energy photonic mode E_{ph1}. (b) RCWA simulated reflectivity of the same suspended grating structure but with a refractive index n_X including an excitonic feature modelled with a Lorentz oscillator (more details in Supplement 1, method section). Both photonic modes E_{ph1} and E_{ph2} (blue dashed lines) described in (a), strongly couple with the exciton, creating two sets of lower (LP), and upper (UP) polaritonic dispersions: (LP_1, UP_1), pink dashed lines, and (LP_2, UP_2), red dashed lines. The BIC in (a) also strongly couples with the exciton giving rise to two polariton-BICs (pol-BICs) in pink. Some excitons (E_X green dashed lines) remain uncoupled to the photonic modes (E_{ph1}, E_{ph2}) and can be seen as a horizontal green dashed line. (c) Polaritonic dispersions of (b) obtained using the photonic modes parameters in (a) and the model in Eq. (2), with E_X = 1.98 eV and V = 90 meV.

Let us now consider a similar suspended grating with an excitonic material of refractive index n_X modeled with a Lorentz oscillator (more details in Supplement 1, method section). Figure 1(b)

Optics EXPRESS

shows the sketch, refractive index, and RCWA reflectivity simulation of this suspended grating. In this structure, the two photonic modes strongly couple to the excitons leading to two sets of polaritonic dispersions (LP_1, UP_1) in pink, and (LP_2, UP_2) in red, with LP for lower polariton, and UP for upper polariton. The excitons interact with each grating mode individually due to the difference of their electric field distribution symmetries in the grating (see Supplement 1, Figs. S3 and S4). This allows us to model this situation as the excitons coupling to each mode independently with the following four-level Hamiltonian from [41]:

$$H_{polaritons} = \begin{pmatrix} E_{ph1}(k_x) & V & 0 & 0 \\ V & E_X & 0 & 0 \\ 0 & 0 & E_{ph2}(k_x) & V \\ 0 & 0 & V & E_X \end{pmatrix} \tag{2}$$

where $E_{ph1}(k_x)$ and $E_{ph2}(k_x)$ are the two dispersions of the uncoupled photonic modes, E_X the exciton energy, and V the coupling strength between the exciton and the photonic modes (here E_X=1.98 eV, and V=90 meV). The exciton states which do not overlap with the photonic modes near-field distributions are not taken into account in this model as they do not contribute to the strong coupling but can be observed in the reflectivity simulations as a flat dispersion (in green).

From Fig. 1(b), one can observe that the exciton E_X is simultaneously strongly coupled with the bright state E_{ph2} and the BIC seen in the photonic mode E_{ph1}, giving rise to two polariton-BICs (pol-BICs) [10] observable on the polaritonic dispersions LP_1, and UP_1.

To further study the double-polaritonic system, RCWA simulations were performed on the suspended gratings for different detunings, $\delta = E_0 - E_X$, between the photonic modes and the exciton energy by changing the grating thickness. Figure 2 presents the RCWA simulations of the suspended grating without an exciton ((a-c), n=4.5) and the excitonic suspended grating ((d-f), $n = n_X$) for grating thicknesses of 15, 20 and 25 nm (a=360 nm, FF=0.8) such that the excitonic energy is either below (a,d), in between (b,e), or above (c,f) the two uncoupled photonic modes. The parameters used to fit the photonic and polaritonic modes are given in Supplement 1, Fig. S5.

When the exciton is below the two photonic modes in the exciton-less gratings ($E_X < E^0_{ph1} < E^0_{ph2}$ with $E^0_{ph1,ph2} = E_0 \pm U$) in Fig. 2(a),(d), the crossing between the exciton energy E_X and the photonic mode E_{ph1} leads to a well defined set of polaritons (LP_1, UP_1) with an anticrossing behavior and a Rabi splitting, $\hbar\Omega = 2V$, of 180 meV. The interaction between the exciton at energy E_X and the uncoupled photonic mode E_{ph2} leads to a set of polaritons (LP_2, UP_2) much closer respectively to the uncoupled exciton energy and the uncoupled photonic mode E_{ph2}. Nevertheless, the coupling strength V of 90 meV is still strong enough for one to discern the polariton dispersions. Moreover, the BIC mode on E_{ph1} for the exciton-less suspended grating in Fig. 2(a) strongly couples with the exciton giving rise to two pol-BICs in the excitonic suspended grating in Fig. 2(d).

The case of the suspended gratings with an exciton above the two photonic modes ($E^0_{ph1} < E^0_{ph2} < E_X$) shown in Figs. 2(c,f), is similar to the previous case. The exciton state here is in resonance with the photonic mode E_{ph2} and is above the photonic mode E_{ph1}. This leads to a well defined polariton set (LP_2, UP_2) with an anticrossing and a Rabi splitting, $\hbar\Omega = 2V$, of 180 meV. However, in this case the upper polariton UP_1 is very close to the flat dispersion (in green) of the uncoupled excitons while having low contrast, which makes it difficult to be discerned.

Finally, when the exciton lies in the gap between the two photonic modes ($E^0_{ph1} < E_X < E^0_{ph2}$) in Figs. 2(b,e), the exciton line does not cross any of the two photonic modes. However, thanks to the high coupling strength V of 90 meV, the two polariton sets (LP_1, UP_1) and (LP_2, UP_2) are well defined and far enough away from the uncoupled exciton flat dispersion to be easily

Optics EXPRESS

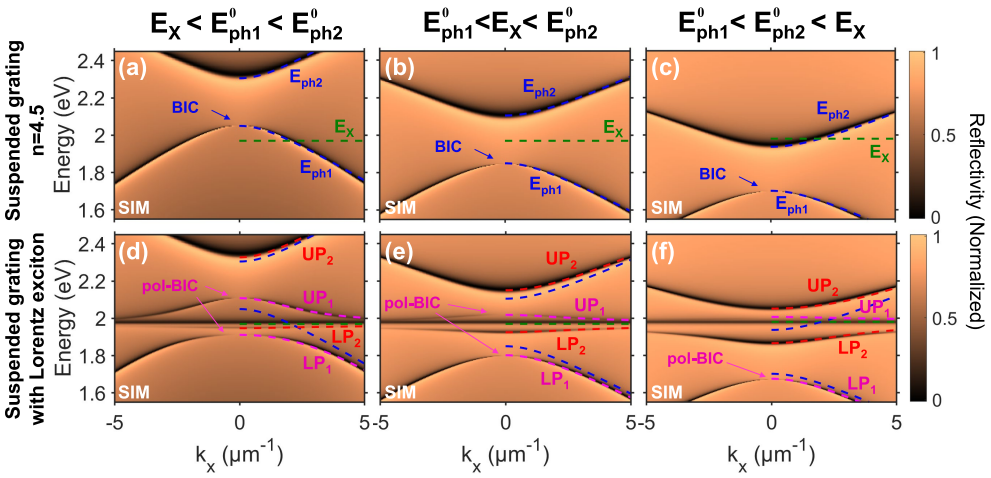

Fig. 2. Numerical simulations of a double polaritonic system in the suspended gratings with different detunings. (a)-(c) RCWA reflectivity simulations of the suspended grating with constant refractive index (n=4.5, k=0) shown in Fig. 1(a) for grating thickness of (a) 15 nm, (b) 20 nm, and (c) 25 nm. The increase of the thickness redshifts the grating photonic modes E_{ph1} and E_{ph2} such that the excitonic energy E_X lies below ($E_X<E^0_{ph1}<E^0_{ph2}$, (a)), in between ($E^0_{ph1}<E_X<E^0_{ph2}$, (b)), or above ($E^0_{ph1}<E^0_{ph2}<E_X$, (c)) the two photonic modes. BICs can be observed on the lower energy photonic modes E_{ph1}. (d)-(f), RCWA reflectivity simulations of the suspended grating with an exciton-like refractive index shown in Fig. 1(b), with respectively the same grating thicknesses as in (a)-(c), and hence with same detunings between the grating photonic modes (E_{ph1}, E_{ph2}) and the exciton E_X. The strong coupling between the exciton and the grating photonic modes with different detunings lead to different double polaritonic systems described by the model in Eq. (2). The parameters used to fit the photonic and polaritonic modes are given in Supplement 1, Fig. S5. The first polaritonic set (LP_1, UP_1) are shown as pink dashed lines, and the second (LP_2, UP_2) as red dashed lines. The BICs in (a)-(c) also strongly couple with the exciton giving rise to polariton-BICs (pol-BICs) indicated in pink. Some excitons (E_X green dashed lines) remain uncoupled to the photonic modes (E_{ph1}, E_{ph2}) and can be seen as horizontal lines in (d)-(f).

resolved. Moreover, the BIC of the exciton-less suspended grating in 2(b,e) strongly couple with the exciton giving rise to two pol-BICs in the excitonic suspended grating Fig. 2(e).

Optics EXPRESS

3. Experimental results

The double-polaritonic system as a function of the detuning was then studied experimentally in six 1D WS_2-based gratings on SiO_2/Si and Au/Si substrates (see Fig. 3). The fabrication is detailed in the method section of Supplement 1 and the microscope and AFM images of the six structures are shown in Supplement 1, Figs. S7 and S8. Figure 4 shows the angle-resolved reflectance contrast measurement (left panels) of the gratings using a spatial-filtering Fourier set-up (more details in Supplement 1, method section), and their matching RCWA simulations (right panels) using the WS_2 refractive index from [34]. The period a of these gratings were 400 nm (350 nm in Fig. 4(a)) and filling factor FF around 0.7 for the grating on SiO_2/Si substrates in Figs. 4(a)-(c) and 0.55 on Au/Si substrates in Figs. 4(d)-(f). The thicknesses of the grating are such that the WS_2 exciton energy either lies below (a, d), in between (b, d), or above (c, f) the two uncoupled photonic modes. The measured and simulated geometrical parameters of the gratings are given in Supplement 1, Fig. S11, while the photonic and polaritonic modes fitting parameters are given in Supplement 1, Fig. S12.

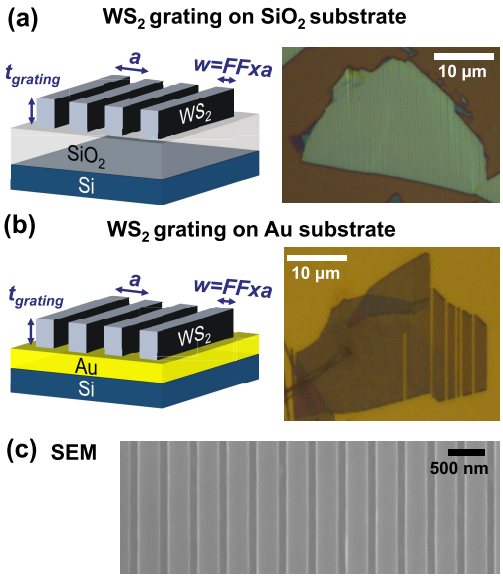

Fig. 3. Experimental WS_2-based 1D gratings. (a),(b) Sketch of the WS_2 gratings respectively on SiO_2/Si (a) and Au/Si (b) substrates along with a microscope images of two of the gratings. The period a of these gratings are 350-400 nm with the filling factors FF around 0.7 for the gratings on SiO_2/Si substrates and 0.55 on Au/Si substrates. (c) Scanning electron microscope (SEM) image of one of the gratings on SiO_2/Si substrate. The optical microscope images, AFM images and measured geometrical parameters of all the structures are shown in Supplement 1, Figs. S7-S11.

From Fig. 4, we first observe that compared to the SiO_2 substrate, the Au substrate improves the reflectivity contrast of the modes but adds losses due to absorption, and flattens the dispersions due the low Au refractive index (≈0.25 at 600 nm). However, we note that our TE modes in s-polarization on Au substrate are not affected with plasmonic effects as they occur under p-polarization. Indeed, plasmonic effect can only be observed on simulated electric field distribution maps of TM modes in a WS_2 grating on Au substrate similar to the one in Fig. 4(f) (see Supplement 1, Fig. S13).

As for the numerical suspended grating, when the exciton lies below the two photonic modes ($E_X < E^0_{ph1} < E^0_{ph2}$) in Fig. 4(a),(d), the polariton set (LP_1, UP_1) presents a well defined anticrossing

Optics EXPRESS

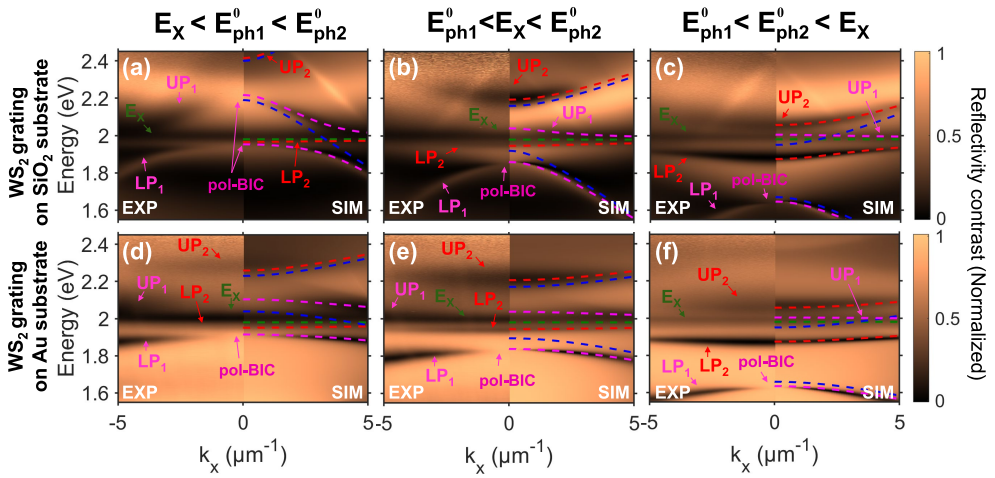

Fig. 4. Double polaritonic system in the WS_2 gratings on SiO_2 and Au substrate with different detunings. Angle-resolved reflectivity contrast measurements (left panels) and RCWA numerical simulations (right panels) of the gratings on SiO_2/Si (a)-(c) and Au/Si (d)-(f) subtrates in the case when $E_X < E^0_{ph1} < E^0_{ph2}$ (a),(d), $E^0_{ph1} < E_X < E^0_{ph2}$ (b),(e), and $E^0_{ph1} < E^0_{ph2} < E_X$ (c),(f). The experimental polaritonic and excitonic dispersions are fitted with the model in Eq. (2) and the resulting dispersions, including the uncoupled photonic dispersions, are plotted on the right pannels for each structures. The photonic and polaritonic modes fitting parameters are given in Supplement 1, Fig. S12. The photonic mode dispersions E_{ph1} and E_{ph2} are plotted as blue dashed line, the WS_2 exciton energy E_X as a green dash line, the polaritonic dispersions $LP_{1(2)}$ and $UP_{1(2)}$ as pink(red) dashed lines, and the polariton-BICs (pol-BICs) are indicated in pink.

with Rabi-splittings, $\hbar\Omega = 2V$, of 160 (a) and 180 (d) meV. Moreover, one can simultaneously observe two pol-BICs on the lower and upper polaritons LP_1, and UP_1 in the case of the grating on the SiO_2 substrate in Fig. 4(a). When the exciton lies above the two photonic modes ($E^0_{ph1} < E^0_{ph2} < E_X$) in Figs. 4(c,f), it is the polariton set (LP_2, UP_2) which is well defined and Rabi splittings of 160 meV.

However, for both cases, due to the losses from the WS_2 absorption and the broader WS_2 exciton, the polariton modes are much broader. Consequently, the complementary polariton sets cannot be fully observed as one of the polariton dispersions (LP_2 in Figs. 4(a,d), UP_1 in Figs. 4(c,f)) are masked by the flat dispersion of the uncoupled excitons.

When the exciton lies within the gap between the two photonic modes ($E^0_{ph1} < E_X < E^0_{ph2}$) for the gratings on SiO_2 and Au subtrates in Figs. 4(b,e), one can easily observe three polaritonic dispersions: LP_1, LP_2, and UP_2 thanks to the large coupling strengths of 85 (b) and 90 (e) meV. However, unlike the simulated suspended grating in Fig. 3(e), the polariton dispersion UP_1 is difficult to be seen due to the WS_2 absorption and the broader uncoupled exciton flat dispersion. Indeed, the upper polariton dispersion is located in the tail of the uncoupled excitonic line.

To reveal the upper polariton UP_1 when the exciton is within the photonic gap ($E^0_{ph1} < E_X < E^0_{ph2}$), reflectance contrast spectra at different wavevectors k_x were further studied in the case of the gratings on Au substrate. The experimental reflectance contrast of Fig. 4(e) is reproduced in Fig. 5(a) with vertical dashed lines of different colors corresponding to the studied spectra. From these slices shown in Fig. 5(b), one can easily observe the reflectivity dips of the polariton dispersions LP_1, LP_2, and UP_2, as well as the uncoupled WS_2 exciton. However, one can observe that for large wavevectors k_x, the linewidth of the uncoupled exciton reflectivity dip broadens for

Optics EXPRESS

energies higher than 2 eV, which corresponds to the hidden upper polariton UP_1 located in the tail of the uncoupled exciton.

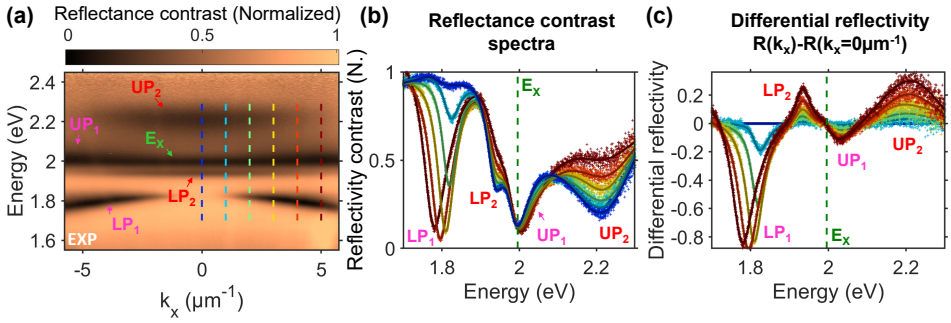

Fig. 5. Differential reflectivity spectra revealing UP_1 polaritons. (a) Experimental reflectivity contrast of the WS_2 grating on Au substrate shown in Fig. 4(e) with vertical dashed lines corresponding to the slices further studied in (b),(c). The different polaritonic dispersions LP_1, LP_2, and UP_2 are indicated with an arrow as well as the last polaritonic dispersion UP_1 located at the tail of the uncoupled exciton absorption. (b) Slices of the reflectivity map for wavevectors k_x from 0 to 5 μm^{-1} indicated by the dashed lines in (a). (c) Differential reflectivity of the slices compared to the slice at $k_x = 0\,\mu m^{-1}$ where the polaritonic dispersions LP_1, LP_2, and UP_2 are well defined. In these differential reflectivity slices, the uncoupled exciton contribution is removed due to the flatness of its dispersion, which reveals the previously unresolvable upper polariton UP_1.

To confirm this hypothesis, we plot in Fig. 5(c) the difference between these spectra at different wavevectors and the spectrum at $k_x = 0$ in order to remove the uncoupled exciton contribution. Indeed, the contribution of the flat uncoupled excitonic dispersion is constant over the range of measured wavevector k_x, and hence disappears in the differential spectra in Fig. 5(c). Similarly to the reflectivity spectra in Fig. 5(b), the polaritonic features LP_1, LP_2 and UP_2 are well defined in such differential reflectivity spectra in Fig. 5(c). More importantly, as the contribution of the uncoupled exciton is removed, one can observe an additional differential reflectivity dip for each spectrum corresponding to the previously unresolvable upper polariton UP_1. Consequently, the two sets of polaritons (LP_1, UP_1) and (LP_2, UP_2) can be experimentally observed simultaneously for the gratings in the case when the exciton lies within the grating photonic gap.

The precense of the upper polariton UP_1 is further numerically confirmed for the structures shown in Figs. 4(b),(e) by using their matching RCWA simulation. Indeed, as shown in Supplement 1, Fig. S14, the previously unresolvable upper polariton UP_1 can be observed from the RCWA simulations of the structure shown in Figs. 4(b),(e), when the reflectance contrast signal is obtained when considering an uppaterned flake as a reference, which removes the contribution of the uncoupled excitons. Then, the numerical example of the suspended gratings, alongside the experimental results and matching RCWA simulations confirm the double polaritonic system in the WS_2-based gratings.

Finally, we note that the Rabi splitting reported here at room temperature are much larger than the ones from photonic structure based on III-V semiconductors with Rabi splittings in the order of a few to ten meV at cryogenic temperatures [7,16,17], or the SiN and Ta_2O_5 gratings coupled respectively with WSe_2 [28] and $MoSe_2$ [15] monolayers with Rabi splitting around 20 meV also at cryogenic temperature. The Rabi splittings are, however, of the same order of magnitude as the ones reported in perovskite-based photonic crystals ranging from 150 meV to 210 meV [9–11] and larger than the previously demonstrated polaritons in quasi-bulk WS_2 gratings with Rabi splittings of 100 meV [39], 120 meV [14], and 170 meV (without the plasmonic mode) [13].

Optics EXPRESS

However, in these WS_2 gratings, the strong coupling was demonstrated with only one of the grating modes and polariton-BICs were not observed.

4. Conclusion

In conclusion, we have presented a highly tunable and versatile platform for the observation of a double polaritonic system based on the quasi-bulk van der Waals excitonic material. In 1D gratings made of the quasi-bulk WS_2, a double polaritonic system was demonstrated with large Rabi splittings ranging from 160 to 180 meV for different detunings of the system, in which the WS_2 excitons are simultaneously strongly coupled with the two grating photonic modes including the Bound State in the Continuum (BIC) of the lower energy mode giving rise to polariton-BICs (pol-BICs).

By using quasi-bulk TMDs, and combining the various advantages of 2D materials and polaritons, we believe that bulk 2D materials can open the way to new polaritonic photonic devices. Indeed, bulk 2D materials, used directly as photonic bulding blocks, have useful properties to offer the fields of nanophotonics such as their large variety of transmission windows with low losses, high refractive indices, excitonic properties, and their compatibility with standard lithography and etching techniques. Moreover, the TMDs offer a versatility in choice of substrate such as demonstrated in this article.

On the other hand, exciton-polaritons have also been attracting interest for photonic device applications as they inherit properties from both their light and matter counterparts. By combining bulk 2D materials and exciton-polaritons, a new direction in polaritonics can be instigated. Finally, using the transferability of TMDs, the highly tunable subwavelength gratings presented in our work could also be used in conjunction with slabs and whole photonic integrated circuits made from van der Waals or many other materials such as III-V membranes. Placing these gratings on top of such photonic structures could thus open the way to 3D nanophotonic heterointegration and straightforward fabrication of sophisticated polaritonic devices.

Funding. Engineering and Physical Sciences Research Council (EP/V026496/1, EP/S030751/1, EP/V006975/1, EP/V007696/1, EP/V047663/1); Royal Academy of Engineering (RF/201718/17131).

Disclosures. The authors declare no conflicts of interest.

Data availability. Data underlying the results presented in this paper are not publicly available at this time but may be obtained from the authors upon reasonable request.

Supplemental document. See Supplement 1 for supporting content.

References

1. C. Weisbuch, M. Nishioka, A. Ishikawa, *et al.*, "Observation of the coupled exciton-photon mode splitting in a semiconductor quantum microcavity," Phys. Rev. Lett. **69**(23), 3314–3317 (1992).
2. J. Kasprzak, M. Richard, S. Kundermann, *et al.*, "Bose-einstein condensation of exciton polaritons," Nature **443**(7110), 409–414 (2006).
3. N. Landau, D. Panna, S. Brodbeck, *et al.*, "Two-photon pumped exciton-polariton condensation," Optica **9**(12), 1347–1352 (2022).
4. E. Maggiolini, L. Polimeno, F. Todisco, *et al.*, "Strongly enhanced light-matter coupling of monolayer ws2 from a bound state in the continuum," Nat. Mater. **22**(8), 964–969 (2023).
5. V. Ardizzone, F. Riminucci, S. Zanotti, *et al.*, "Polariton bose-einstein condensate from a bound state in the continuum," Nature **605**(7910), 447–452 (2022).
6. F. Riminucci, A. Gianfrate, D. Nigro, *et al.*, "Polariton condensation in gap-confined states of photonic crystal waveguides," Phys. Rev. Lett. **131**(24), 246901 (2023).
7. J. Hu, N. Lydick, Z. Wang, *et al.*, "Grating-based microcavity with independent control of resonance energy and linewidth for non-Hermitian polariton system," Appl. Phys. Lett. **121**(8), 081106 (2022).
8. E. Khestanova, V. Shahnazaryan, V. K. Kozin, *et al.*, "Electrostatic control of nonlinear photonic-crystal polaritons in a monolayer semiconductor," Nano Lett. **24**(24), 7350–7357 (2024).
9. X. Wu, S. Zhang, J. Song, *et al.*, "Exciton polariton condensation from bound states in the continuum at room temperature," Nat. Commun. **15**(1), 3345 (2024).
10. N. H. M. Dang, S. Zanotti, E. Drouard, *et al.*, "Realization of polaritonic topological charge at room temperature using polariton bound states in the continuum from perovskite metasurface," Adv. Opt. Mater. **10**(6), 2102386 (2022).

Optics EXPRESS

11. S. Kim, B. H. Woo, S.-C. An, *et al.*, "Topological control of 2d perovskite emission in the strong coupling regime," Nano Lett. **21**(23), 10076–10085 (2021).
12. Y. Wang, J. Tian, M. Klein, *et al.*, "Directional emission from electrically injected exciton-polaritons in perovskite metasurfaces," Nano Lett. **23**(10), 4431–4438 (2023).
13. H. Zhang, B. Abhiraman, Q. Zhang, *et al.*, "Hybrid exciton-plasmon-polaritons in van der waals semiconductor gratings," Nat. Commun. **11**(1), 3552 (2020).
14. X. Zong, L. Li, and Y. Liu, "Photonic bound states in the continuum in nanostructured transition metal dichalcogenides for strong photon–exciton coupling," Opt. Lett. **46**(24), 6095–6098 (2021).
15. V. Kravtsov, E. Khestanova, F. A. Benimetskiy, *et al.*, "Nonlinear polaritons in a monolayer semiconductor coupled to optical bound states in the continuum," Light: Sci. Appl. **9**(1), 56 (2020).
16. P. Gagel, O. A. Egorov, F. Dzimira, *et al.*, "An electrically pumped topological polariton laser," Nano Lett. **24**(22), 6538–6544 (2024).
17. P. St-Jean, V. Goblot, E. Galopin, *et al.*, "Lasing in topological edge states of a one-dimensional lattice," Nat. Photonics **11**(10), 651–656 (2017).
18. T. Kuriakose, P. M. Walker, T. Dowling, *et al.*, "Few-photon all-optical phase rotation in a quantum-well micropillar cavity," Nat. Photonics **16**(8), 566–569 (2022).
19. T. Gao, P. S. Eldridge, T. C. H. Liew, *et al.*, "Polariton condensate transistor switch," Phys. Rev. B **85**(23), 235102 (2012).
20. H. S. Nguyen, D. Vishnevsky, C. Sturm, *et al.*, "Realization of a double-barrier resonant tunneling diode for cavity polaritons," Phys. Rev. Lett. **110**(23), 236601 (2013).
21. C. Sturm, D. Tanese, H. S. Nguyen, *et al.*, "All-optical phase modulation in a cavity-polariton mach-zehnder interferometer," Nat. Commun. **5**(1), 3278 (2014).
22. F. Marsault, H. S. Nguyen, D. Tanese, *et al.*, "Realization of an all optical exciton-polariton router," Appl. Phys. Lett. **107**(20), 201115 (2015).
23. S. W. Lee, J. S. Lee, W. H. Choi, *et al.*, "Ultra-compact exciton polariton modulator based on van der waals semiconductors," Nat. Commun. **15**(1), 2331 (2024).
24. S.-C. An, Y. Lim, K. Y. Lee, *et al.*, "Topological exciton polaritons in compact perovskite junction metasurfaces," Adv. Funct. Mater. **34**(32), 2313840 (2024).
25. J. Von Neumann and E. Wigner, "Über merkwürdige diskrete Eigenwerte," Z. Phys **30**, 465–497 (1929).
26. H. Friedrich and D. Wintgen, "Interfering resonances and bound states in the continuum," Phys. Rev. A **32**(6), 3231–3242 (1985).
27. R. El-Ganainy, M. Khajavikhan, D. N. Christodoulides, *et al.*, "The dawn of non-hermitian optics," Commun. Phys. **2**(1), 37 (2019).
28. L. Zhang, R. Gogna, W. Burg, *et al.*, "Photonic-crystal exciton-polaritons in monolayer semiconductors," Nat. Commun. **9**(1), 713 (2018).
29. M. Li, I. Sinev, F. Benimetskiy, *et al.*, "Experimental observation of topological z2 exciton-polaritons in transition metal dichalcogenide monolayers," Nat. Commun. **12**(1), 4425 (2021).
30. B. Munkhbat, A. B. Yankovich, D. G. Baranov, *et al.*, "Transition metal dichalcogenide metamaterials with atomic precision," Nat. Commun. **11**(1), 4604 (2020).
31. T. Isoniemi, P. Bouteyre, X. Hu, *et al.*, "Realization of z2 topological photonic insulators made from multilayer transition metal dichalcogenides," ACS Nano **18**(47), 32547–32555 (2024).
32. A. A. Vyshnevyy, G. A. Ermolaev, D. V. Grudinin, *et al.*, "van der waals materials for overcoming fundamental limitations in photonic integrated circuitry," Nano Lett. **23**(17), 8057–8064 (2023).
33. B. Munkhbat, P. Wróbel, T. J. Antosiewicz, *et al.*, "Optical constants of several multilayer transition metal dichalcogenides measured by spectroscopic ellipsometry in the 300-1700 nm range: High index, anisotropy, and hyperbolicity," ACS Photonics **9**(7), 2398–2407 (2022).
34. P. G. Zotev, Y. Wang, D. Andres-Penares, *et al.*, "Van der waals materials for applications in nanophotonics," Laser Photonics Rev. **17**(8), 2200957 (2023).
35. H. Ling, A. Manna, J. Shen, *et al.*, "Deeply subwavelength integrated excitonic van der waals nanophotonics," Optica **10**(10), 1345–1352 (2023).
36. S. A. Randerson, P. G. Zotev, X. Hu, *et al.*, "High q hybrid mie-plasmonic resonances in van der waals nanoantennas on gold substrate," ACS Nano **18**(25), 16208–16221 (2024).
37. B. Munkhbat, D. G. Baranov, M. Stührenberg, *et al.*, "Self-hybridized exciton-polaritons in multilayers of transition metal dichalcogenides for efficient light absorption," ACS Photonics **6**(1), 139–147 (2019).
38. T. Weber, L. Kühner, L. Sortino, *et al.*, "Intrinsic strong light-matter coupling with self-hybridized bound states in the continuum in van der waals metasurfaces," Nat. Mater. **22**(8), 970–976 (2023).
39. H. Cho, D.-J. Shin, J. Sung, *et al.*, "Ultra-thin grating coupler for guided exciton-polaritons in ws2 multilayers," Nanophotonics **12**(13), 2563–2571 (2023).
40. H. Ling, R. Li, and A. R. Davoyan, "All van der waals integrated nanophotonics with bulk transition metal dichalcogenides," ACS Photonics **8**(3), 721–730 (2021).
41. H. Sigurðsson, H. C. Nguyen, and H. S. Nguyen, "Dirac exciton–polariton condensates in photonic crystal gratings," Nanophotonics **13**(18), 3503–3518 (2024).